Eur. Phys. J. E **29**, 275–284 (2009)
DOI 10.1140/epje/i2009-10484-8

THE EUROPEAN PHYSICAL JOURNAL E

Regular Article

Contact mechanics and rubber friction for randomly rough surfaces with anisotropic statistical properties

G. Carbone[1,2,a], B. Lorenz[1,3], B.N.J. Persson[1], and A. Wohlers[3]

[1] IFF, FZ-Jülich, D-52425 Jülich, Germany
[2] DIMeG - Politecnico di Bari, v.le Japigia 182, 70126 Bari, Italy
[3] IFAS, RWTH Aachen University, D-52074 Aachen, Germany

Received 21 February 2009
Published online: 4 July 2009 –

Abstract. In this paper we extend the theory of contact mechanics and rubber friction developed by one of us (B.N.J. Persson, J. Chem. Phys. **115**, 3840 (2001)) to the case of surfaces with anisotropic surface roughness. As an application we calculate the viscoelastic contribution to the rubber friction. We show that the friction coefficient may depend significantly on the sliding direction, while the area of contact depends weakly on the sliding direction. We have carried out experiments for rubber blocks sliding on unidirectionally polished steel surfaces. The experimental data are in a good qualitative agreement with the theory.

PACS. 46.55.+d Tribology and mechanical contacts – 81.40.Pq Friction, lubrication, and wear – 62.40.+i Anelasticity, internal friction, stress relaxation, and mechanical resonances – 81.05.Lg Polymers and plastics; rubber; synthetic and natural fibers; organometallic and organic materials

1 Introduction

The interaction between two contacting solids plays a major role in a large number of physical phenomena and engineering applications, *e.g.* structural adhesives, protective coatings, friction of tires, lubrication, wear and seals, but still is not completely understood. As an example, there have been many attempts to explain the proportionality between the applied load and the contact area. The explanation given by Bowden and Tabor in 1939 [1] holds true only when plastic flow occurs at the interfaces of the approaching solids. However, in many engineering situations the contact is purely elastic [2], and the above explanation does not apply. As an example, wear experiments suggests that contact of asperities is formed under elastic rather than plastic deformations: when machine parts slide against each other for perhaps millions of cycles, the protuberances may be plastically deformed at the beginning, but soon reach a steady-state condition in which the load is supported elastically, thus avoiding serious damage to the machine. In these cases, after a short run-in time period, plastic deformation is very limited, and elastic deformations play a major role [2].

In the case of rubber materials (*e.g.* tires and seals), plastic deformations often do not occur, and the area of intimate contact is therefore determined by the viscoelastic properties of the material [3,4], the surface energies of the contacting bodies and their roughness [5,6]. In all such situations the simple explanation given by Bowden and Tabor does not work.

In the last decades, a great deal of research has been carried out in order to gain a better understanding of friction and contact mechanics [7–13]. In 2001 Persson [14] proposed a novel theory to predict adhesion and friction between a viscoelastic solid and a rough rigid substrate. The theory was developed for randomly rough surfaces with statistical properties which are translational invariant and isotropic (*i.e.*, rotational invariant), for which the surface power spectral density (PSD) $C(\mathbf{q})$ depends on the wave vector $\mathbf{q}$ only through its module $q = |\mathbf{q}|$. In such cases, the friction coefficient and the contact area cannot, of course, depend on the sliding direction, and although many surface of practical interest have surface roughness with statistical properties which are actually isotropic (*e.g.* asphalt surfaces or sand-blasted surfaces) many others are not. As an example, unidirectional polished surface may have strongly anisotropic statistical properties, and therefore should also present frictional properties that strongly depend on the direction of sliding.

The aim of this paper is, hence, to extend Persson's theory in such a way that it can handle also surfaces with anisotropic statistical properties. As an application we calculate the viscoelastic contribution to the rubber friction. We show that the sliding direction has a relatively strong

[a] e-mail: carbone@poliba.it

influence on the friction coefficient, but affects much less the contact area. The theoretical results are in good agreement with experiments we carry out with the aid of an *ad hoc* testing machine, under temperature-controlled conditions. We note, however, that in addition to the hysteretic contribution to the rubber friction we calculate, there may also be an adhesional contribution which depends on the area of real contact. The latter contribution may originate from the propagation of opening cracks [15], or from stick-slip motion of nanometer-sized rubber volume element (stress domains) at the rubber-substrate interface [16].

2 Contact mechanics for rough surfaces with anisotropic statistical properties

Consider a viscoelastic slab sliding at constant velocity $\mathbf{v}$ on a rigid rough surface with anisotropic statistical properties. Let $\sigma(\mathbf{x},t)$ and $u(\mathbf{x},t)$ be the normal stress and elastic displacement at the interface of the two contacting bodies. Since the viscoelastic solid slides at constant velocity, we can write $\sigma(\mathbf{x},t) = \sigma(\mathbf{x}-\mathbf{v}t)$ and $u(\mathbf{x},t) = u(\mathbf{x}-\mathbf{v}t)$. In Fourier space we obtain

$$\sigma(\mathbf{q},\omega) = \frac{1}{(2\pi)^3}\int \mathrm{d}^2x\mathrm{d}t\ \sigma(\mathbf{x},t)e^{-i(\mathbf{q}\cdot\mathbf{x}-\omega t)} = \sigma(\mathbf{q})\delta(\omega-\mathbf{q}\cdot\mathbf{v}), \quad (1)$$

$$u(\mathbf{q},\omega) = \frac{1}{(2\pi)^3}\int \mathrm{d}^2x\mathrm{d}t\ u(\mathbf{x},t)e^{-i(\mathbf{q}\cdot\mathbf{x}-\omega t)} = u(\mathbf{q})\delta(\omega-\mathbf{q}\cdot\mathbf{v}), \quad (2)$$

where

$$\sigma(\mathbf{q}) = \frac{1}{(2\pi)^2}\int \mathrm{d}^2x\ \sigma(\mathbf{x},t)e^{-i\mathbf{q}\cdot\mathbf{x}}, \quad (3)$$

$$u(\mathbf{q}) = \frac{1}{(2\pi)^2}\int \mathrm{d}^2x\ u(\mathbf{x},t)e^{-i\mathbf{q}\cdot\mathbf{x}}. \quad (4)$$

For a viscoelastic material the Fourier transforms of the normal stresses σ and the normal displacement u can be shown to be related to each other by

$$\sigma(\mathbf{q},\omega) = M^{-1}(\mathbf{q},\omega)u(\mathbf{q},\omega), \quad (5)$$

where $M^{-1}(\mathbf{q},\omega)$ is the inverse of the response function of the viscoelastic solid. Now, let us assume that the sliding velocity $v = |\mathbf{v}|$ is negligible compared to the speed of sound c in the solid, as is the case in most cases of practical interest. This is equivalent to assuming that the rate ω of deformation in the viscoelastic material is small compared to qc. Under this assumption it can be shown (see appendix A) that the response function of a linear viscoelastic isotropic material $M(\mathbf{q},\omega)$ can be written in the form

$$M(\mathbf{q},\omega) = -\frac{2[1-\nu^2(\omega)]S(|\mathbf{q}|d)}{E(\omega)|\mathbf{q}|}, \quad (6)$$

where d is the thickness of the viscoelastic slab and the real function $S(|\mathbf{q}|d)$ is a correction factor which accounts for different constraint or boundary conditions. For a semi-infinite solid (*i.e.* $d\to\infty$) the corrective factor is $S(|\mathbf{q}|h)=1$. In eq. (6) we have assumed that the Poisson ratio $\nu(\omega)$ is frequency dependent, but in the applications below we assume that we can neglect this frequency dependence.

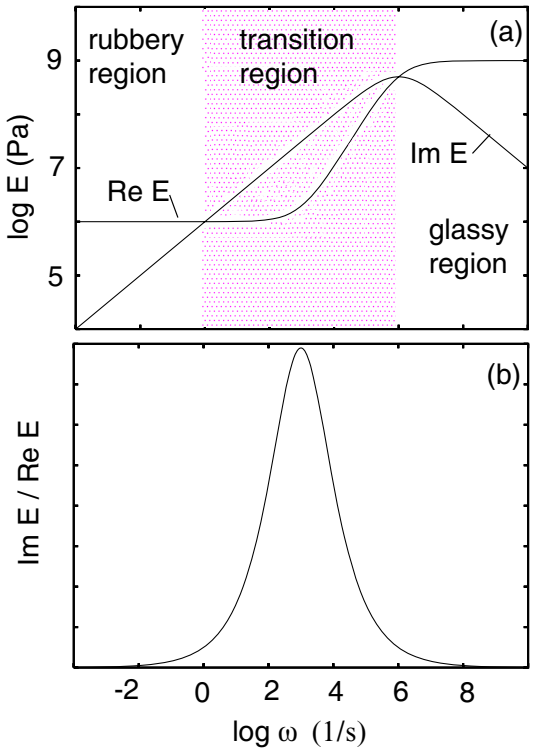

Fig. 1. (a) The viscoelastic modulus $E(\omega) = E_1 + iE_2$ of a typical rubber-like material, and (b) the loss tangent E_2/E_1. The latter quantity is maximal at some frequency ω_2.

Figure 1 shows the general structure of the viscoelastic modulus $E(\omega)$ of rubber-like materials. The real part $\mathrm{Re}\,E(\omega)$, the imaginary part $\mathrm{Im}\,E$ of $E(\omega)$ and the loss tangent $\mathrm{Im}\,E/\mathrm{Re}\,E(\omega)$ are shown. At "low" frequencies the material is in the so-called "rubbery" region where $\mathrm{Re}\,E(\omega)$ is relatively small and approximately constant, and where the loss tangent $\mathrm{Im}\,E/\mathrm{Re}\,E(\omega)$ rapidly decreases to zero as the angular frequency ω is reduced to zero. Indeed, in the "rubbery" region the solid behaves as if it were perfectly elastic with negligible energy dissipation. At very high frequencies the material is instead very stiff (brittle-like). In this "glassy" region $\mathrm{Re}\,E$ is again nearly constant but is much larger (typically by 3 orders of magnitude) than in the rubbery region. Note that in this region the loss tangent $\mathrm{Im}\,E/\mathrm{Re}\,E(\omega)$ is again very small, so that in the "glassy" region the solid behaves as a (stiff) perfectly elastic material. At intermediate frequencies, in the so-called "transition" region, the loss tangent is very large and it is mainly this region which determines, *e.g.*, the friction when a tire is sliding on a road surface.

The physical origin of the frequency dependence of the dynamical modulus $E(\omega)$ for rubber-like materials is related to stress-aided, thermally activated flipping of

polymer segments between different configurations. If τ denotes the typical flipping time, then for $\omega \gg 1/\tau$ there is no time for thermally activated rearrangement of the polymer chain segments to occur, and the rubber response will be that of a hard glassy material. On the contrary, when $\omega \ll 1/\tau$, thermal activated rearrangements of the rubber polymer chains will occur adiabatically, resulting in a soft elastic rubbery response. The frequency and temperature dependence of the elastic modulus $E(\omega, T)$ is indeed a function of the form $E \approx E(\omega\tau)$, where τ depends on temperature according to a thermally activated process.

Given eqs. (1) and (2), eq. (5) can be conveniently rephrased as

$$\sigma(\mathbf{q}) = M^{-1}(\mathbf{q}, \mathbf{q}\cdot\mathbf{v})u(\mathbf{q}), \tag{7}$$

which simply states that for a viscoelastic solid sliding at a constant velocity $\mathbf{v}$ the stresses and displacements will be related by a velocity-dependent viscoelastic response function $M^{-1}(\mathbf{q}, \mathbf{q}\cdot\mathbf{v})$. It is worthwhile to observe that in our case $\omega = \mathbf{q}\cdot\mathbf{v}$, and recalling that $|E(\omega)|$ increases with the frequency of the external excitation, we expect the material to become stiffer (resulting in a smaller contact area) as the term $|\mathbf{q}\cdot\mathbf{v}|$ is increased, and also that, in the case of anisotropic surface roughness, the material should behave differently depending on the direction of sliding. Thus, for rubber friction on a uniaxial polished surface the contact area will be larger when sliding along the direction of the wear tracks than when sliding orthogonal to the wear tracks. However, the numerical results presented below show that this effect is rather small, and already a few degrees' deviation in the sliding direction from the wear track direction will result in a contact area nearly identical to that obtained for sliding orthogonal to the wear tracks (see fig. 4).

As already stated, the main purpose here is to extend the theory of friction and contact mechanics developed in ref. [14] by one of the authors (B.N.J.P.), to the case of surfaces with anisotropic statistical properties. These kind of surfaces are often encountered in practical engineering applications, *e.g.* polished surfaces of which the surface roughness has a preferential direction. In order to pursue our aim, we start from the determination of the probability distribution $P(\sigma, \zeta)$ of the normal stress σ in the contact area (at fixed magnification ζ). $P(\sigma, \zeta)$ can be written as

$$P(\sigma, \zeta) = \langle \delta(\sigma - \sigma_1(\mathbf{x}, \zeta))\rangle, \tag{8}$$

where $\sigma_1(\mathbf{x}, \zeta)$ represents the normal stress field in the (apparent) contact area at magnification ζ. By following the same argument as given in ref. [14], we can show that the probability density distribution $P(\sigma, \zeta)$ satisfies the following diffusion equation:

$$\frac{\partial P(\sigma, \zeta)}{\partial \zeta} = f(\zeta)\frac{\partial^2 P(\sigma, \zeta)}{\partial \sigma^2}\,, \tag{9}$$

where the general form of the diffusivity function $f(\zeta)$ is

$$f(\zeta) = \frac{1}{2}\frac{\langle(\Delta\sigma)^2\rangle}{\Delta\zeta}\,. \tag{10}$$

In ref. [14] $f(\zeta)$ is calculated assuming perfect contact between the viscoelastic solid and the rigid rough substrate. Here we follow the same approach to calculate $f(\zeta)$ for anisotropic surfaces. To this end, let us define the stress distribution at the magnification ζ as

$$\sigma(\mathbf{x}, \zeta) = \int_{|\mathbf{q}|<\zeta q_L} \mathrm{d}^2q\; M^{-1}(\mathbf{q}, \mathbf{q}\cdot\mathbf{v})u(\mathbf{q})e^{i\mathbf{q}\cdot\mathbf{x}}, \tag{11}$$

where $q_L = 2\pi/L$ and L is the lateral size of solid block. We can therefore write

$$\Delta\sigma(\mathbf{x}, \zeta) = \int_D \mathrm{d}^2q\; M^{-1}(\mathbf{q}, \mathbf{q}\cdot\mathbf{v})u(\mathbf{q})e^{i\mathbf{q}\cdot\mathbf{x}},$$

where the domain $D = \{\mathbf{q} : \zeta q_L < |\mathbf{q}| < (\zeta + \Delta\zeta)q_L\}$. The quantity $\langle(\Delta\sigma)^2\rangle$ can be determined as

$$\langle(\Delta\sigma)^2\rangle = \int_D\int_D \mathrm{d}^2q\,\mathrm{d}^2q'\; M^{-1}(\mathbf{q}, \mathbf{q}\cdot\mathbf{v}) \times M^{-1}(\mathbf{q}', \mathbf{q}'\cdot\mathbf{v})\langle u(\mathbf{q})u(\mathbf{q}')\rangle e^{i(\mathbf{q}+\mathbf{q}')\cdot\mathbf{x}}. \tag{12}$$

Now recall that, in order to calculate $f(\zeta)$ we are considering full contact conditions, in such a case $u(\mathbf{x}) = h(\mathbf{x})$ just represents the height distribution of the surface roughness, and assuming that the surface roughness is well described by a transitionally invariant statistical process [13] and that the average value of the roughness is $\langle h(\mathbf{x})\rangle = 0$, we end up with the relation

$$\langle u(\mathbf{q})u(\mathbf{q}')\rangle = \delta(\mathbf{q} + \mathbf{q}')C(\mathbf{q}), \tag{13}$$

where

$$C(\mathbf{q}) = \frac{1}{(2\pi)^2}\int \mathrm{d}^2x\; \langle h(\mathbf{x})h(\mathbf{0})\rangle e^{-i\mathbf{q}\cdot\mathbf{x}} \tag{14}$$

is the power spectral density of the surface roughness, which can be easily obtained from the measured height profile (see appendix B). Equation (12) then becomes

$$\langle(\Delta\sigma)^2\rangle = \int_D \mathrm{d}^2q|M^{-1}(\mathbf{q}, \mathbf{q}\cdot\mathbf{v})|^2 C(\mathbf{q}) \tag{15}$$

and in polar coordinates

$$\langle(\Delta\sigma)^2\rangle = \int_q^{q+\Delta q} \mathrm{d}q q \times \int_0^{2\pi} \mathrm{d}\theta \left|M^{-1}(\mathbf{q}, \mathbf{q}\cdot\mathbf{v})\right|^2 C(\mathbf{q}), \tag{16}$$

where $q = |\mathbf{q}| = \zeta q_L$ and $\Delta q = q_L\Delta\zeta$. Thus we obtain

$$\langle(\Delta\sigma)^2\rangle = \left(q\int_0^{2\pi} \mathrm{d}\theta \left|M^{-1}(\mathbf{q}, \mathbf{q}\cdot\mathbf{v})\right|^2 C(\mathbf{q})\right) q_L\Delta\zeta, \tag{17}$$

from which it follows that

$$f(\zeta) = \frac{1}{2}\frac{\langle(\Delta\sigma)^2\rangle}{\Delta\zeta} = \frac{1}{2}qq_L\int_0^{2\pi} \mathrm{d}\theta \left|M^{-1}(\mathbf{q}, \mathbf{q}\cdot\mathbf{v})\right|^2 C(\mathbf{q}). \tag{18}$$

Using eq. (6) we obtain the general form of the diffusivity function valid for anisotropic surfaces.

$$f(\zeta) = \frac{1}{8} q_L q^3 \int_0^{2\pi} \mathrm{d}\theta \; C(\mathbf{q}) \left| \frac{E(\mathbf{q}\cdot\mathbf{v})}{(1-\nu^2)S(qd)} \right|^2 . \quad (19)$$

We define the quantity

$$G(q) = \frac{1}{8} \int_{q_L}^{q} \mathrm{d}q' q'^3 \times \int_0^{2\pi} \mathrm{d}\theta \; C(\mathbf{q}') \left| \frac{E(\mathbf{q}'\cdot\mathbf{v})}{(1-\nu^2)S(q'd)\sigma_0} \right|^2 , \quad (20)$$

which is related to $f(\zeta)$ trough $f(\zeta) = \sigma_0^2 \mathrm{d}G/\mathrm{d}\zeta = q_L \sigma_0^2 G'(q)$, were σ_0 is the mean pressure on the nominal contact area A_0, *i.e.* $\sigma_0 = F/A_0$ with F being the normal applied load. Once the function $f(\zeta)$ or equivalently $G(q)$ is determined, it is possible, by following the same procedure as outlined in ref. [14], to determine the apparent area of contact $P(q) = A(q)/A_0$ at the magnification $\zeta = q/q_L$ as

$$P(q) = \int_0^{\infty} \mathrm{d}\sigma P(\sigma, \zeta) = \mathrm{erf}\left(\frac{1}{2\sqrt{G(q)}} \right) \quad (21)$$

and also to calculate the friction coefficient

$$\mu = \frac{1}{2} \int \mathrm{d}^2q \; q\hat{v}\cdot\mathbf{q} C(\mathbf{q}) P(q) \, \mathrm{Im} \, \frac{E(\mathbf{q}\cdot\mathbf{v})}{(1-\nu^2)S(q'd)\sigma_0} , \quad (22)$$

where $\mathbf{v}$ is the sliding velocity, $\hat{v} = \mathbf{v}/v$ is a unit vector along the sliding direction. We note that in deriving this equation we have neglected the influence of the adhesional interaction between the surfaces. However, if the roughness is large enough, adhesion will only manifest itself at high magnification (corresponding to large wave vectors q in the integral in (22)), and in this case the increase in the hysteretic contribution to the friction from the (adhesion induced) increase in the contact area may be very small. Adhesion can be included in the analysis above if $P(q)$ is calculated including the adhesional interaction [5]. However, this does not account for the contribution to the friction from the energy dissipation at opening cracks and from stick-slip of interfacial rubber volume elements in the area of real contact (see sect. 1).

3 Rubber friction on hard rough surfaces with anisotropic statistical properties

Many surfaces used in engineering have surfaces roughness with anisotropic statistical properties. Thus, for example, a unidirectional polished steel surface will have wear tracks along the polishing direction and the surface roughness power spectrum $C(\mathbf{q})$ of such a surface will depend on the direction of the wave vector $\mathbf{q}$ and not just on its magnitude, as would be the case for surfaces with isotropic statistical properties.

As shown in sect. 2, the rubber friction theory developed in [14] can be easily extended to surfaces with anisotropic statistical properties. Thus the friction coefficient for steady sliding (without the flash temperature effect) is given by

$$\mu = \frac{1}{2} \int \mathrm{d}^2q \; q\hat{v}\cdot\mathbf{q} C(\mathbf{q}) P(q) \, \mathrm{Im} \, \frac{E(\mathbf{q}\cdot\mathbf{v})}{(1-\nu^2)\sigma_0} ,$$

where $\mathbf{v}$ is the sliding velocity, $\hat{v} = \mathbf{v}/v$ is a unit vector along the sliding direction, and where $P(q)$ is the relative contact area when the interface is studied at the resolution $\lambda = 2\pi/q$ (see sect. 2). The nominal pressure (or perpendicular stress) σ_0 at the sliding interface is assumed to be constant. We can write

$$P(q) = \mathrm{erf}\left(\frac{1}{2\sqrt{G(q)}} \right) ,$$

where

$$G(q) = \frac{1}{8} \int_{q_L}^{q} \mathrm{d}^2q \; q^2 C(\mathbf{q}) \left| \frac{E(\mathbf{q}\cdot\mathbf{v})}{(1-\nu^2)\sigma_0} \right|^2 .$$

If the sliding occurs along the x-axis,

$$\mu = \frac{1}{2} \int \mathrm{d}^2q \; qq_x C(\mathbf{q}) P(q) \, \mathrm{Im} \, \frac{E(q_x v)}{(1-\nu^2)\sigma_0} .$$

If the sliding occurs along the y-axis one must replace q_x with q_y.

Experimental studies of rubber friction on surfaces with anisotropic statistical properties could be interesting for testing theories of rubber friction because the adhesional contribution to the rubber friction may be nearly independent of the sliding direction (because the area of real contact depends weakly on the sliding direction, see below), while the hysteresis contribution could change drastically. For example, for 1D surface roughness the hysteresis contribution would vanish when sliding along the direction where the height profile is constant. Of course, even a unidirectional polished surface will exhibit some roughness along the polishing direction, so in practice some hysteresis contribution to the rubber friction will always remain independent of the sliding direction and the system under study.

Let us illustrate the theory with rubber friction on a polished steel surface. Figure 2 shows the kinetic friction coefficient as a function of the logarithm (with 10 as basis) of the sliding velocity, for several angles α between the sliding direction and the x-axis, which is perpendicular to the polishing direction. The results are for a tread rubber compound in contact with a unidirectionally polished steel surface, with the (angular averaged) power spectrum shown in fig. 9 (red curve). In the calculation we have used the full power spectrum $C(\mathbf{q})$ (not shown), which depends not only on $q = |\mathbf{q}|$ but also on the direction in the $\mathbf{q}$-plane. $C(\mathbf{q})$ was obtained using the 2D Fast Fourier Transform as applied to the height profile $h(\mathbf{x}) = h(x, y)$ measured using an optical method. In the calculation we only include the roughness components with wave vector $1 \times 10^6 \, \mathrm{m}^{-1} < |\mathbf{q}| < 2 \times 10^8 \, \mathrm{m}^{-1}$, since $C(\mathbf{q})$ was not measured for larger (or smaller) q. For the same system, fig. 3

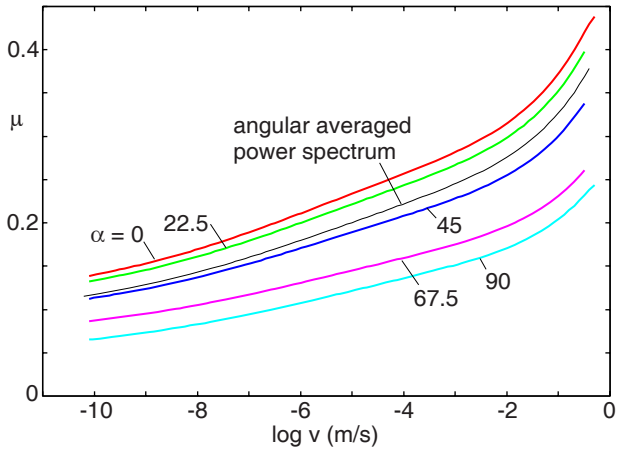

Fig. 2. The kinetic friction coefficient as a function of the logarithm (with 10 as basis) of sliding velocity, for several angles α (in degrees) between the sliding direction and the x-axis, which is perpendicular to the polishing direction. We also show the friction which results from using the angular-averaged power spectrum (thin black line). The results are for a tread rubber compound on a unidirectionally polished steel surface with the power spectrum shown in fig. 9 (red curve).

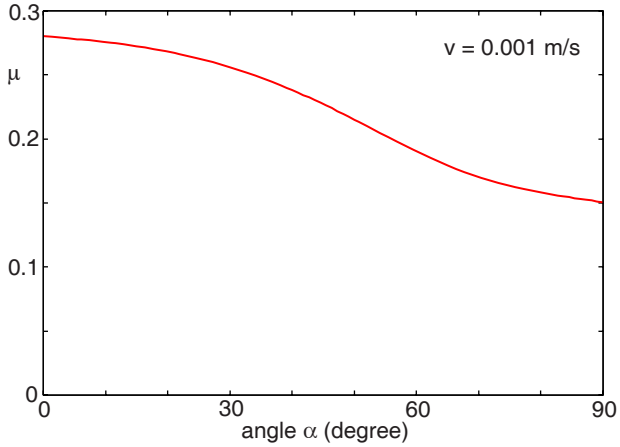

Fig. 3. The kinetic friction coefficient as a function of the angle α between the sliding direction and the x-axis, which is perpendicular to the polishing direction. Same system as in fig. 2, for a sliding velocity of 0.001 m/s.

shows the kinetic friction coefficient as a function of the angle α, when the sliding velocity is 0.001 m/s. Finally, in fig. 4 we show the (projected) contact area (in units of the nominal contact area A_0), as a function of the logarithm of the sliding velocity. Note that for $0 < \alpha < 67.5$ the contact area is nearly independent of α. Hence, for these cases we do expect a negligible α-dependence of the contribution to the friction from the area of real contact. The decrease in the contact area with increasing sliding velocity (see fig. 4) is due to the increase in the frequencies of the dynamical deformation of the rubber with increasing sliding velocity. Thus, an asperity contact region with diameter d will give rise to pulsating deformations acting on the rubber surface and characterized by the frequency $\omega = v/d$.

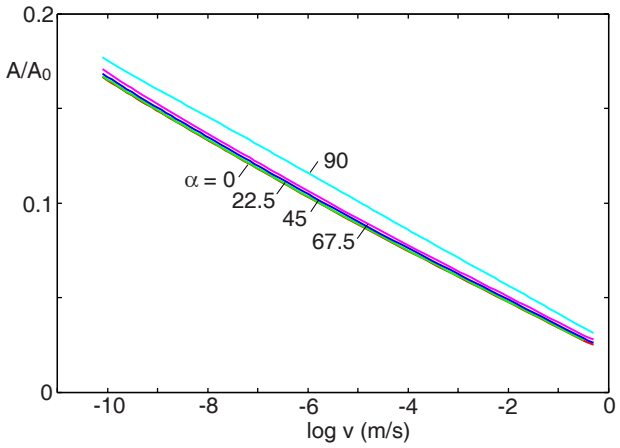

Fig. 4. The (projected) contact area (in units of the nominal contact area A_0), as a function of the logarithm (with 10 as basis) of sliding velocity, for several angles α (in degrees) between the sliding direction and the x-axis, which is perpendicular to the polishing direction. Same system as in fig. 2.

Since the (absolute value of the) rubber elastic modulus increases with increasing frequency ω, it follows that the contact area will decrease with increasing sliding velocity. At high sliding velocity (typically above 0.001 m/s) frictional heating of the rubber will be important, and this in turn could result in an increase in the contact area with increasing sliding velocity (as observed in simulations of rubber friction in the context of tire dynamics), but here we are interested in the simpler case (from the point of view of testing the theory) where the velocity is so low that this effect can be neglected.

4 Experiment and results

We slide a rubber block against an anisotropic, randomly rough steel surface. The substrate was prepared by unidirectional grinding with a surface grinding machine. This is a state-of-the-art technique in many engineering applications to reduce the roughness at flat surfaces. To the naked eye the surface appears smooth, but looking more closely one observes numerous wear tracks induced by the silicide-carbide particles of the grinding disc. The rubber block is made from a tread rubber where the exact composition is not known to us.

We put a well-defined load on the rubber block using a dead weight, and then slide it over the anisotropic steel surface with a constant pulling force. The present study was performed with the nominal (squeezing) pressure ≈ 0.1 MPa and at the temperature $T = 17\,^{\circ}$C. We obtain the sliding velocity v from the time needed for the rubber samples to travel a certain distance (we assume that v is constant over the distance measured). We vary the direction of sliding relative to the direction of the wear tracks of the substrate; the angle between the direction orthogonal to the wear tracks and the sliding direction is denoted by α. Dividing the pulling force with the normal force gives the coefficient of friction as a function of v, α,

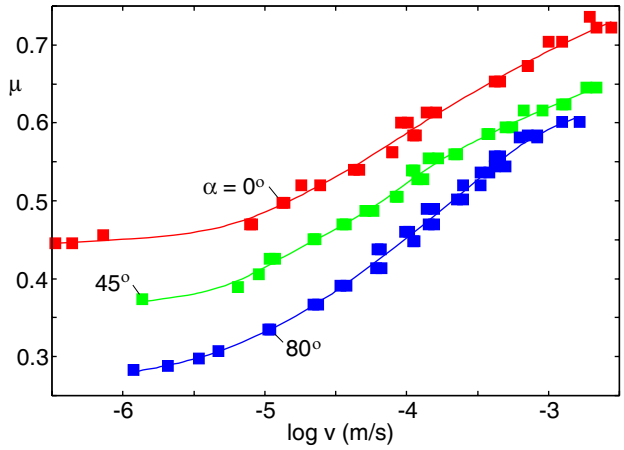

Fig. 5. The square symbols are the measured relation between the friction coefficient and the sliding velocity for three angles $\alpha = 0°$, 45° and 80° between the sliding direction and the direction orthogonal to the polishing direction. The solid lines are a guide for the eye. The tread rubber block sliding experiment on a unidirectional polished steel surface was done at a nominal squeezing pressure 0.1 MPa and temperature $T = 17\,°\mathrm{C}$.

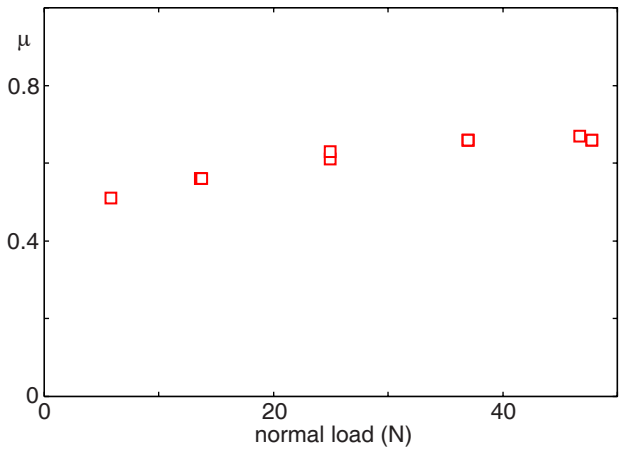

Fig. 6. The friction coefficient μ as a function of the normal force for $\alpha = 0°$ between the sliding direction and the direction orthogonal to the polishing direction. The velocity of the tread rubber block was kept constant at about 0.2 mm/s. The figure shows a very weak load dependence of the friction coefficient.

normal force F_N and temperature T. Here we only report on the dependence of μ on v and α (a detailed study of the dependence of μ on all the variables v, α, F_N and T will be presented elsewhere).

Before starting the experiment, it is crucial to first run in the rubber samples properly. Within this run-in, a thin skin-layer on the rubber surface as well as dirt particles from the production process and from the normal atmosphere will be removed and a boundary layer (thin layer of modified properties) is formed on the rubber surface. It is important to run in the rubber at the highest velocity with the highest friction coefficient, thereby forming a relative thick boundary layer which (hopefully) does not change very much during the following tests at lower sliding speed and normal load. Between the experiments the steel surface was carefully cleaned with a mixture of 10% acetylacetone in isopropanol.

In fig. 5 we show the measured friction coefficient as a function of the logarithm of the sliding speed, for three angles $\alpha = 0$, 45° and 80°. For these angles the theory predicts that the area of real contact will be nearly the same (see fig. 4) so the dependence of the friction on the angle α is likely to be due to the variation of the hysteretic contribution alone. At high velocities the 80° curve increases stronger than it should. This is due to the fact that the slider starts to tilt a little bit because of the shear forces pulling it into the direction of grinding. We plan to improve the set-up and will report on more complete results elsewhere. The measurement is for a different tread rubber and a different (but similarly prepared) substrate than the one used in the model calculation presented in sect. 3, and we cannot compare the results in fig. 5 quantitatively with the calculation in fig. 2, but the qualitative agreement is good. In the calculation presented in fig. 2 we only included surface roughness over slightly more than 2 decades in length scales. Including the roughness at longer and shorter length scales will increase the calculated friction, making it closer to the observed values. Roughness on other length scales may also change the velocity dependence somewhat, and may explain why the difference between the calculated friction coefficients for different α increases with increasing sliding velocities, while the opposite is the case in the experiment. An alternative explanation is that perhaps there is another non-negligible contribution to the friction from energy dissipation during crack opening [17] which exhibits a different velocity dependence than the roughness-induced hysteretic contribution discussed above. A detailed comparison of theory with experiment for the present system will be presented elsewhere. However, we have carried out an additional experiment (see fig. 6), which shows that, for the case under study, the friction coefficient μ has a very weak dependence on the applied normal load. If adhesion manifested itself on a macroscopic scale as a finite pull-off force, the friction coefficient would decrease with increasing load, whereas fig. 6 shows that the friction coefficient slightly increases with normal load.

5 Summary and conclusion

The existing theory of contact mechanics and friction developed by one of us (B.N.J.P.) [14] is based on the assumption that the averaged two-dimensional PSD does not deviate from the one-dimensional PSDs for different measurement directions and is therefore only valid for isotropic surfaces. Many surfaces of practical relevance in engineering applications have anisotropic statistical properties and cannot be properly managed by the existing theory. Therefore in this paper we have extended the theory to the case of anisotropic surfaces. We have shown that the friction coefficient may depend significantly on the sliding direction, while the area of contact depends weakly on it. To confirm the theory, we have carried out

experiments with rubber blocks sliding on unidirectionally grinded steel surfaces. We have shown some experimental results for three different sliding directions where we have varied the velocity in a range of about four decades. The experimental results are in good qualitative agreement with the theory. We plan to improve the test rig to eliminate the observed tilting effect, and measure the viscoelastic properties of the rubber and the statistical properties of surface roughness. Thereby a quantitative comparison of theory and experiment can be done. The present extension of the theory to anisotropic surfaces may be very important in many technical applications since surface anisotropy is usually a direct consequence of surface treatment process.

This work, as part of the European Science Foundation EUROCORES Programme FANAS was supported from the EC Sixth Framework Programme, under contract N. ERAS-CT-2003-980409.

Appendix A. The viscoelastic response function

For a viscoelastic material the equation of motion can be written in the form

$$\rho\frac{\partial^2\mathbf{u}}{\partial t^2}(\mathbf{x},t)=\int_{-\infty}^{\infty}\mathrm{d}\tau\,\mu(t-\tau)\nabla^2\mathbf{u}(\mathbf{x},\tau)+\int_{-\infty}^{\infty}\mathrm{d}\tau\,[\mu(t-\tau)+\lambda(t-\tau)]\nabla\nabla\cdot\mathbf{u}(\mathbf{x},\tau),\qquad(A.1)$$

where $\mathbf{u}=(u_x,u_y,u_z)$ and where $u_z=u$. Of course because of causality, the quantities μ and λ satisfy the relations $\mu(t)=0$ and $\lambda(t)=0$ for $t<0$. Here we are interested to the long-term steady motion of the solid so that taking the time Fourier transform we get

$$-\omega^2\rho\mathbf{u}(\mathbf{x},\omega)=\mu(\omega)\nabla^2\mathbf{u}(\mathbf{x},\omega)+[\mu(\omega)+\lambda(\omega)]\nabla\nabla\cdot\mathbf{u}(\mathbf{x},\omega),\qquad(A.2)$$

where we have defined

$$\mu(\omega)=\int_0^{\infty}\mathrm{d}t\;\mu(t)e^{i\omega t},$$
$$\lambda(\omega)=\int_0^{\infty}\mathrm{d}t\;\lambda(t)e^{i\omega t}.$$

Now let us define the complex viscoelastic modulus and $E(\omega)$ and the Poisson ratio $\nu(\omega)$ through the relations

$$\lambda(\omega)=\frac{\nu(\omega)E(\omega)}{[1+\nu(\omega)][1-2\nu(\omega)]}\,,\qquad(A.3a)$$

$$\mu(\omega)=\frac{E(\omega)}{2[1+\nu(\omega)]}\,,\qquad(A.3b)$$

and substituting in eq. (A.1) we have

$$-\omega^2\rho\frac{2[1+\nu(\omega)]}{E(\omega)}\mathbf{u}(\mathbf{x},\omega)=\nabla^2\mathbf{u}(\mathbf{x},\omega)+\frac{1}{1-2\nu(\omega)}\nabla\nabla\cdot\mathbf{u}(\mathbf{x},\omega).\qquad(A.4)$$

Assuming that the quantity $|\dot{\mathbf{u}}|$ is negligible in comparison to the sound speed in the solid we can neglect the inertia term and recover the standard Navier equation for a viscoelastic solid

$$\nabla^2\mathbf{u}(\mathbf{x},\omega)+\frac{1}{1-2\nu(\omega)}\nabla\nabla\cdot\mathbf{u}(\mathbf{x},\omega)=0.\qquad(A.5)$$

Equations (A.2) and (A.3) show that there is an analogy between elastic and viscoelastic problems, in that the viscoelastic deformations of the solid can be readily derived in the ω-space from the corresponding elastic solution by simply substituting the elastic modulus and the Poisson ratio with the frequency-dependent analogues quantities $E(\omega)$ and $\nu(\omega)$. This analogy is often referred to as the elastic-viscoelastic correspondence principles, although in order to hold true it is necessary that at every point of the solid surface the boundary conditions does not change from traction to displacement specification [18]. Now we can proceed to determine the response function $M(\mathbf{q},\omega)$ for three cases which most often are of interest for engineering applications.

Semi-infinite solid

Consider a semi-infinite elastic solid. The response function we are looking for can be simply derived by Fourier transforming the displacement field $u(\mathbf{x})=u_z(\mathbf{x})$ determined by the application of a concentrated load $\delta(\mathbf{x})$ on the free surface of the solid block (*i.e.* by Fourier transforming the corresponding Green function). The solution of this problem was given for the first time by Boussinesq (1985)

$$u(\mathbf{x})=-\frac{1-\nu^2}{2\pi E}\frac{1}{|\mathbf{x}|}\,.\qquad(A.6)$$

Thus taking the Fourier transform of eq. (A.6) we can easily determine $M(\mathbf{q})$ as

$$M(\mathbf{q})=\int\mathrm{d}^2x\;u(\mathbf{x})e^{-i\mathbf{q}\cdot\mathbf{x}}=-2\frac{(1-\nu^2)}{E|\mathbf{q}|}\,.\qquad(A.7)$$

If the solid is viscoelastic the elastic-viscoelastic correspondence principle allows us to write

$$M(\mathbf{q},\omega)=-2\frac{1-\nu^2(\omega)}{E(\omega)|\mathbf{q}|}\,.\qquad(A.8)$$

Thick slab

Now let us consider an elastic slab of thickness d sandwiched between a flat rigid plate (upper part) and a rough substrate (bottom part), as shown in fig. 7(a). For such a case, in ref. [19] the response function for the elastic case has been calculated, therefore enforcing the correspondence principle we get for the linear viscoelastic case

$$M(\mathbf{q},\omega)=-2\frac{1-\nu^2(\omega)}{E(\omega)}\frac{1}{q}\times\frac{(3-4\nu)\sinh(2qd)-2qd}{(3-4\nu)\cosh(2qd)+2(qd)^2-4\nu(3-2\nu)+5}\,,\qquad(A.9)$$

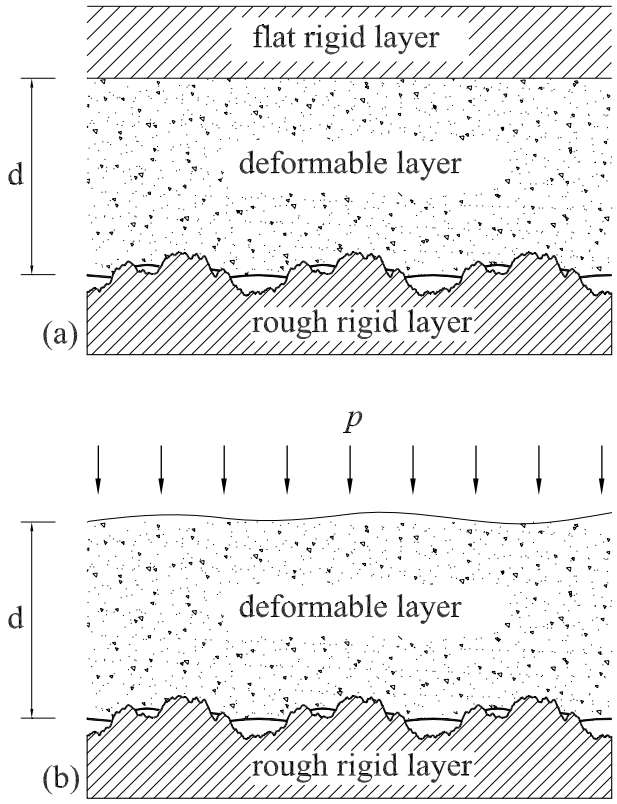

Fig. 7. A deformable layer of thickness d in contact with a rough substrate. The layer is assumed to be glued to the upper plate (a), or subjected to a uniform applied pressure p (b).

where $q = |\mathbf{q}|$. If we instead consider the situation depicted in fig. 7(b), where the thick slab is subjected to a uniform applied pressure, by following the same argument outlined in ref. [19] and making use of the elastic-viscoelastic correspondence principle, we can easily derive the following viscoelastic response function as:

$$M(\mathbf{q},\omega) = -2\frac{1-\nu^2(\omega)}{E(\omega)}\frac{1}{q}\frac{\sinh(2qd)+2qd}{\cosh(2qd)-2(qd)^2-1}\,. \tag{A.10}$$

We observe that for different constraints or boundary conditions we can always write, for an isotropic viscoelastic solid,

$$M(\mathbf{q},\omega) = -2\frac{1-\nu^2(\omega)}{E(\omega)}\frac{S(qd)}{q}\,, \tag{A.11}$$

where $S(qd)$ is a correction factor. Observe that in both cases letting $qd \to \infty$ we recover eq. (A.7). Also it is worthwhile to note that when $qh \gtrapprox 4$, in both cases the correction factor deviates from the unit value less than 10%.

Appendix B. Relation between the 1D and 2D power spectrum

We consider randomly rough surfaces where the statistical properties are transitionally invariant, but not necessarily isotropic. In this case complete information about the statistical properties of the surface is, in general, only obtained by measuring the height profile over a square (or rectangular) surface area, *i.e.*, a single line scan does, in general, not contain the full information about the statistical properties of the surface. In particular, the 2D power spectrum $C_{2\mathrm{D}}(\mathbf{q}) = C(\mathbf{q})$ cannot, in general, be obtained from the 1D power spectrum $C_{1\mathrm{D}}(q)$. However, for the limiting cases of (a) isotropic surface roughness and (b) 1D surface roughness, the 2D power spectrum can be obtained from the 1D power spectrum. Isotropic surface roughness may prevail for, *e.g.*, surfaces prepared by sand blasting, while 1D surface roughness may result from polishing if the direction of polishing is fixed. Since some experimental techniques measure the surface topography only along line scans, rather than over rectangular surface areas, it is important to be able to calculate $C_{2\mathrm{D}}(\mathbf{q})$ from $C_{1\mathrm{D}}(q)$. For the two limiting cases discussed above, this can be done as follows:

2D isotropic surface roughness

In this case the 2D power spectrum will only depend on the magnitude q of the wave vector $\mathbf{q}$. Consider the definition

$$C_{2\mathrm{D}}(\mathbf{q}) = \frac{1}{(2\pi)^2}\int \mathrm{d}^2x\ \langle h(\mathbf{x})h(\mathbf{0})\rangle e^{-i\mathbf{q}\cdot\mathbf{x}}. \tag{B.1}$$

We also have

$$\langle h(\mathbf{x})h(\mathbf{0})\rangle = \int_{-\infty}^{\infty}\mathrm{d}q'\ C_{1\mathrm{D}}(q')e^{iq'|\mathbf{x}|}.$$

Substituting this in (B.1) gives

$$C_{2\mathrm{D}}(q) = \frac{1}{(2\pi)^2}\int \mathrm{d}^2x\int_{-\infty}^{\infty}\mathrm{d}q'\ C_{1\mathrm{D}}(q')e^{i(q'|\mathbf{x}|-\mathbf{q}\cdot\mathbf{x})}.$$

Let us choose the x-axis along the $\mathbf{q}$-direction so that $\mathbf{q}\cdot\mathbf{x} = qr\cos\phi$, where we have introduced polar coordinates in the $\mathbf{x}$-plane so that $x = r\cos\phi$. Thus

$$\begin{aligned}C_{2\mathrm{D}}(q) &= \frac{1}{(2\pi)^2}\int_{-\infty}^{\infty}\mathrm{d}q'\ C_{1\mathrm{D}}(q')\int \mathrm{d}^2x\ e^{i(q'-q\cos\phi)r}\\ &= \frac{1}{2\pi^2}\int_0^{\infty}\mathrm{d}q'\ C_{1\mathrm{D}}(q')\,\mathrm{Re}\int_0^{2\pi}\mathrm{d}\phi\int_0^{\infty}\mathrm{d}r r\ e^{i(q'+q\cos\phi)r}\\ &= \frac{1}{2\pi^2}\int_0^{\infty}\mathrm{d}q'\,C_{1\mathrm{D}}(q')\,\mathrm{Re}\,\frac{1}{i}\frac{\mathrm{d}}{\mathrm{d}q'}\int_0^{2\pi}\mathrm{d}\phi\int_0^{\infty}\mathrm{d}r\,e^{i(q'+q\cos\phi)r}.\end{aligned}$$

In order to be able to perform the r-integral, we add a factor $\exp(-\epsilon r)$, where ϵ is a small (infinitesimal) positive number. We get

$$\begin{aligned}C_{2\mathrm{D}}(q) = \frac{1}{2\pi^2}&\int_0^{\infty}\mathrm{d}q'\ C_{1\mathrm{D}}(q')\\ &\times\frac{\mathrm{d}}{\mathrm{d}q'}\,\mathrm{Re}\int_0^{2\pi}\mathrm{d}\phi\ \frac{1}{q'+q\cos\phi+i\epsilon}\,.\end{aligned}$$

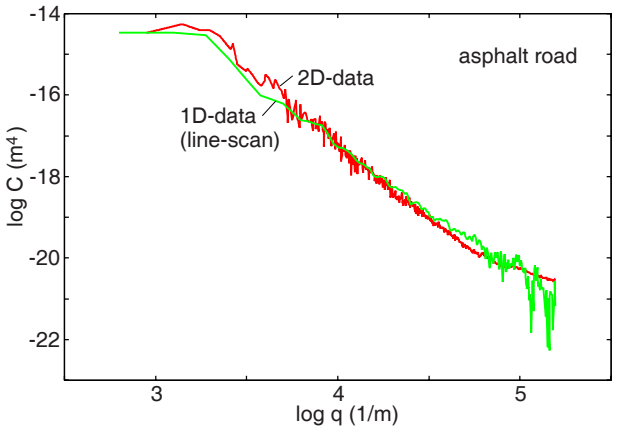

Fig. 8. (Colour on-line) The 2D surface roughness power spectrum $C_{2D} = C(q)$ for an asphalt road surface obtained from 2D data (red curve) and from 1D data (line scan) (green curve). In the latter case we have averaged over 500 different line scans. The surface has the root-mean-square roughness ≈ 0.3 mm.

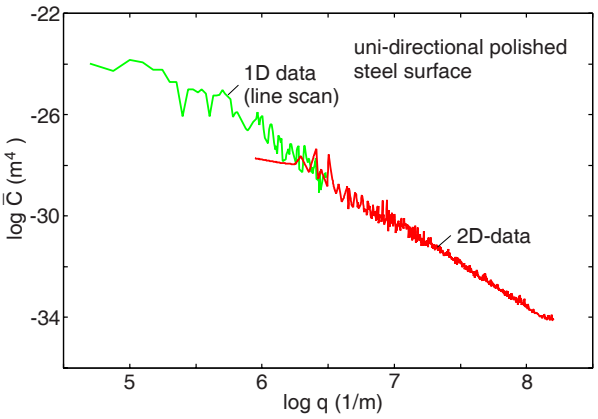

Fig. 9. (Colour on-line) The angular-average of the 2D surface roughness power spectrum $\bar{C}_{2D}(q)$ for a unidirectional polished steel surface obtained from 2D data (red curve), and from 1D data (line scan) (green curve) obtained at lower resolution (corresponding to smaller wave vectors). The root-mean-square roughness is $\approx 0.08\,\mu$m from the 2D data and $\approx 0.5\,\mu$m from the 1D line scan data. The surface topography of the 2D data is shown in fig. 10.

Performing a partial integration over q' gives

$$C_{2D}(q) = \frac{1}{2\pi^2}\int_0^\infty dq'\ [-C'_{1D}(q')] \times \mathrm{Re}\int_0^{2\pi} d\phi\ \frac{1}{q' + q\cos\phi + i\epsilon}\,.$$

The integration over ϕ is standard: write $z = \exp(i\phi)$ and perform the integral over z by summing up the contributions from the poles located inside the unit circle in the complex z-plane. This gives after some simplifications

$$C_{2D}(q) = \frac{1}{\pi}\int_q^\infty dq' \frac{[-C'_{1D}(q')]}{(q'^2 - q^2)^{1/2}}\,. \qquad \text{(B.2)}$$

This equation is a very convenient way of obtaining C_{2D} from 1D line scans of the surface topography. In fig. 8 we show the 2D surface roughness power spectrum $C_{2D} = C(q)$ for an asphalt road surface obtained from 2D-data (red curve) and from 1D-data (line scan) (green curve). In the latter case we have averaged over 500 different line scans. The surface has the root-mean-square roughness ≈ 0.3 mm.

1D surface roughness

If we choose the y-axis along the direction where $h(\mathbf{x})$ is constant, we get $h(\mathbf{x}) = h(x, 0)$ and (B.1) becomes

$$C_{2D}(\mathbf{q}) = \frac{1}{2\pi}\int dx\ \langle h(x,0)h(0,0)\rangle e^{-iq_x x} \times \frac{1}{2\pi}\int dy\ e^{-iq_y y} = C_{1D}(q_x)\delta(q_y).$$

In many application the angular average of $C_{2D}(\mathbf{q})$ enters, which only depends on the magnitude q of the wave vector,

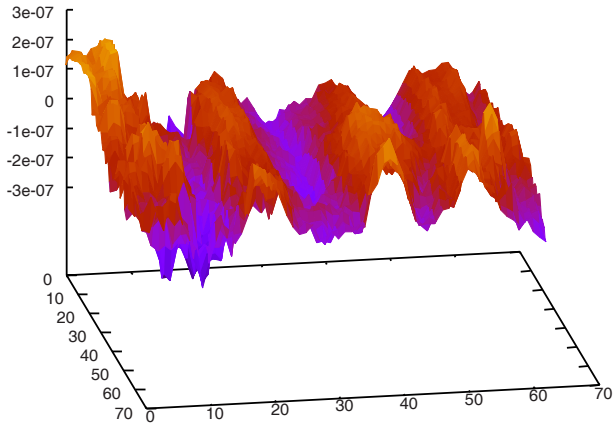

Fig. 10. The surface topography of the 2D data used in calculating the red curve in fig. 9. Surface area $10\,\mu\text{m} \times 10\,\mu$m.

and which becomes

$$\bar{C}_{2D}(q) = \frac{1}{2\pi}\int_0^{2\pi} d\phi\ C_{2D}(\mathbf{q}) = \frac{1}{2\pi}\int_0^{2\pi} d\phi\ C_{1D}(q\cos\phi)\delta(q\sin\phi) = \frac{C_{1D}(q)}{\pi q}\,, \qquad \text{(B.3)}$$

where we have used that $\delta(q\sin\phi) = [\delta(\phi) + \delta(\phi - \pi)]/q$. In fig. 9 we show the angular average of the 2D surface roughness power spectrum $\bar{C}_{2D}(q)$ for a unidirectional polished steel surface obtained from 2D data (red curve), and from 1D data (line scan) (green curve) obtained at lower resolution (corresponding to smaller wave vectors). The root-mean-square roughness is $\approx 0.08\,\mu$m from the 2D data and $\approx 0.5\,\mu$m from the 1D line scan data. The surface topography of the 2D data is shown in fig. 10.

Appendix C. Contact mechanics of 1D rough surfaces and comparison with the 2D case

Here we briefly compare contact mechanics for 1D roughness with 2D roughness. It is impossible to produce surfaces with strict 1D roughness but such surfaces may be of interest when testing contact mechanics theories, because it is possible to perform numerical studies for much larger systems with 1D roughness than for systems with 2D roughness. However, all analytical contact mechanics theories are of the mean-field type and it is known that mean-field theories in general become more accurate as the spatial dimension increases.

According to the theory presented in sect. 2, for elastic solids with randomly rough surfaces with translational invariant statistical properties, the normalized contact area is given by

$$P(q) = \mathrm{erf}\left(\frac{1}{2\sqrt{G(q)}}\right),$$

where

$$G(q) = \left|\frac{E}{(1-\nu^2)\sigma_0}\right|^2 \frac{1}{8}\int_{q_{\mathrm{L}}}^{q} \mathrm{d}^2q\; q^2 C(\mathbf{q}).$$

Note that

$$\langle[\nabla h(\mathbf{x})]^2\rangle_q = \int_{q_{\mathrm{L}}}^{q} \mathrm{d}^2q\; q^2 C(\mathbf{q}).$$

Thus, we can also write

$$G(q) = \left|\frac{E}{(1-\nu^2)\sigma_0}\right|^2 \frac{1}{8}\langle[\nabla h(\mathbf{x})]^2\rangle_q.$$

This equation is valid also for surfaces with roughness with anisotropic statistical properties. Note that for 1D roughness

$$\langle[\nabla h(\mathbf{x})]^2\rangle = \langle(\partial h/\partial x)^2\rangle.$$

If we now consider 2D roughness with isotropic statistical properties, and assume that the statistical properties of the surface topography along a line is the same as for the 1D roughness case (where the line scan is perpendicular to the surface corrugation), then we have

$$\langle[\nabla h(\mathbf{x})]^2\rangle = \langle(\partial h/\partial x)^2\rangle + \langle(\partial h/\partial y)^2\rangle = 2\langle(\partial h/\partial x)^2\rangle.$$

Since the surface area for small loads is proportional to $G^{-1/2}$, we conclude that *at small loads the contact area for surfaces with* 1D *roughness is larger by a factor of* $\sqrt{2}$ *than for the case of* 2D *roughness, given same statistical properties of the surfaces along line scans.*

References

1. F.P. Bowden, D. Tabor, Proc. R. Soc. London, Ser. A-Math. Phys. Eng. Sci. **169**, 391 (1939).
2. J.F. Archard, W. Hirst, Proc. R. Soc. London, Ser. A-Math. Phys. Eng. Sci. **236**, 397 (1956).
3. B.N.J. Persson, O. Albohr, C. Creton, V. Peveri, J. Chem. Phys. **120**, 8779 (2004).
4. C.Y. Hui, Y.Y. Lin, J.M. Baney, J. Polym. Sci. B **38**, 1485 (2000).
5. B.N.J. Persson, Eur. Phys. J. E **8**, 385 (2002).
6. G. Carbone, L. Mangialardi, B.N.J. Persson, Phys. Rev. B **70**, 125407 (2004).
7. S. Hyun, L. Pei, J.-F. Molinari, M.O. Robbins, Phys. Rev. E **70**, 026117 (2004).
8. M. Borri-Brunetto, B. Chiaia, M. Ciavarella, Comput. Meth. Appl. Mech. Eng. **190**, 6053 (2001).
9. C. Campañà, M.H. Müser, M.O. Robbins, J. Phys.: Condens. Matter **20**, 354013 (2008).
10. B.N.J. Persson, *Sliding Friction: Physical Principles and Applications*, 2nd edition (Springer, Heidelberg, 2000).
11. J.N. Israelachvili, *Intermolecular and Surface Forces* (Academic, London, 1995).
12. B.N.J. Persson, Surf. Sci. Rep. **61**, 201 (2006).
13. B.N.J. Persson, O. Albohr, U. Tartaglino, A.I. Volokitin, E. Tosatti., J. Phys.: Condens. Matter **17**, R1 (2005).
14. B.N.J. Persson, J. Chem. Phys. **115**, 3840 (2001).
15. B.N.J. Persson, O. Albohr, G. Heinrich, H. Ueba, J. Phys.: Condens. Matter **17**, R1071 (2005).
16. A. Schallamach, Wear **6**, 375 (1963); B.N.J. Persson, A.I. Volokitin, Eur. Phys. J. E **21**, 69 (2006).
17. D. Maugis, J. Adhes. Sci. Technol. **9**, 1005 (1995).
18. R.M. Christensen, *Theory of Viscoelasticity*, 2nd edition (Dover Publications, Inc., Mineola, New York, 2003).
19. G. Carbone, L. Mangialardi, J. Mech. Phys. Solids **56**, 684 (2008).